Original Article

Institution of MECHANICAL ENGINEERS
Journal of POWER AND ENERGY

Proc IMechE Part A:
J Power and Energy
2014, Vol. 228(5) 585–591

DOI: 10.1177/0957650914530294
pia.sagepub.com
SAGE

Analysis of silt abrasion and blade shape optimization in a centrifugal pump

Zhongdong Qian[1], Zhiyuan Wang[1], Kai Zhang[1], Yuan Wu[1] and Yulin Wu[2]

Abstract

Water flow and silt movement in a double-suction centrifugal pump were simulated using an Euler–Lagrange multiphase flow model. Blade erosion rates were predicted using a particle erosion model and the influence of inlet and outlet shapes on silt abrasion was analyzed. The results show: the inlet relative velocity is larger on the suction side than on the pressure side; the blade inlet and outlet are severely silt abraded and the average erosion rate is always larger on the suction side than on the pressure side; the inlet relative velocity and the impact angle are two important influencing factors, and can be controlled by changing the inlet and outlet shapes to reduce erosion rate and increase pump efficiency. In this simulation, two effective means of reducing erosion rates are decreasing the hydraulic loss and increasing pump head and pump efficiency.

Keywords

Centrifugal pump, silt abrasion, blade shape, numerical simulation

Date received: 6 August 2013; accepted: 4 March 2014

Introduction

Double-suction centrifugal pumps are widely used in irrigation pumping stations along the Yellow River. Because of high silt content in the Yellow River, the pump impeller is usually severely abraded by silt, resulting in decreases in pump head and pump efficiency. Tang et al.[1] studied three-dimensional (3D) two-phase flow in a Francis turbine runner and predicted blade abrasion. Li et al.[2] studied solid–liquid two-phase turbulent flow in a centrifugal pump and silt abrasion characteristics. Qian et al.[3] studied the effect of silt diameter and silt concentration on the erosion rate of a centrifugal pump blade. Chen et al.[4] studied the effect of splitter blades on the pump flow characteristics.

With the development of computational fluid dynamics (CFD), 3D multiphase flow in pumps has been simulated extensively to predict pump performance and optimize the impeller geometry. CFD has thus become a powerful and effective tool in pump design for industrial applications.[5–8]

In our study, the water flow and movement of silt in a double-suction centrifugal pump were simulated using an Euler–Lagrange multiphase flow model. Blade erosion rates were predicted using a particle erosion model and the influence of inlet and outlet shape on silt abrasion was analyzed. The aim of this paper is to provide some reference methods that suppress silt abrasion of blades.

Physical model

Figure 1 shows the computational domain of the centrifugal pump, which is composed of four parts: inlet, impeller, volute, and outlet. The impeller diameter is 0.765 m, the rotation speed is 960 r/min, and the number of blades is eight. Figure 2 shows a 3D view of the impeller. Because of its complex geometry, an unstructured mesh is employed to discretize the computational domain. The total number of mesh cells is about 3,500,000.

Governing equations

The 3D Reynolds-averaged Navier–Stokes equations for incompressible flow are as follows[9]

$$\frac{\partial \rho}{\partial t} + \frac{\partial}{\partial x_i}(\rho u_i) = 0 \quad (1)$$

[1]State Key Laboratory of Water Resources and Hydropower Engineering Science, Wuhan University, Wuhan, PR China
[2]Department of Thermal Engineering, Tsinghua University, Beijing, PR China

Corresponding author:
Zhongdong Qian, State Key Laboratory of Water Resources and Hydropower Engineering Science, Wuhan University, Wuhan 430072, PR China.
Email: zdqian@whu.edu.cn

$$\frac{\partial(\rho u_i)}{\partial t}+\frac{\partial(\rho u_i u_j)}{\partial x_j}=-\frac{\partial p}{\partial x_i}+\frac{\partial}{\partial x_j}\left(\mu\frac{\partial u_i}{\partial x_j}\right)+\frac{\partial \tau_{ij}}{\partial x_j} \quad (2)$$

where $\tau_{ij}=-\rho\overline{u_i' u_j'}$ is the Reynolds stress.

The $k-\varepsilon$ turbulence model is chosen for equation closure. Considering the rotating flow inside the pump impeller, the renormalization group (RNG) $k-\varepsilon$ model, which is effective for strongly rotating flow, is adopted in this simulation.[10,11]

The equations for turbulence kinetic energy k and dissipation rate ε are

$$\frac{\partial(\rho k)}{\partial t}+\frac{\partial(\rho k u_i)}{\partial x_i}=\frac{\partial}{\partial x_j}\left[\left(\mu+\frac{\mu_t}{\sigma_k}\right)\frac{\partial k}{\partial x_j}\right]+G_k+\rho\varepsilon \quad (3)$$

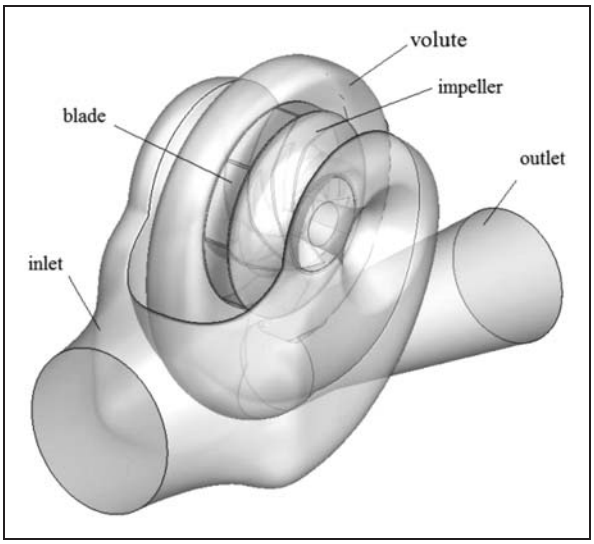

Figure 1. 3D perspective view of the double-suction pump.

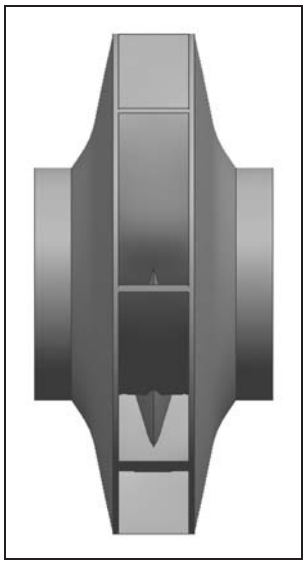

Figure 2. 3D perspective view of the impeller.

$$\frac{\partial(\rho\varepsilon)}{\partial t}+\frac{\partial(\rho\varepsilon u_i)}{\partial x_i}=\frac{\partial}{\partial x_j}\left[\left(\mu+\frac{\mu_t}{\sigma_\varepsilon}\right)\frac{\partial k}{\partial x_j}\right]+\frac{C_{1\varepsilon}^{*}\varepsilon}{k}G_k-C_{2\varepsilon}\rho\frac{\varepsilon^2}{k} \quad (4)$$

where the model constants are chosen from Yakhot and Orszag.[11] For the RNG $k-\varepsilon$ model, the Reynolds stress can be written as

$$\tau_{ij}=\mu_t\left(\frac{\partial u_i}{\partial x_j}+\frac{\partial u_j}{\partial x_i}\right)-\frac{2}{3}\left(\rho k+\mu_t\frac{\partial u_i}{\partial x_i}\right)\delta_{ij} \quad (5)$$

with the turbulence kinetic viscosity coefficient given by

$$\mu_t=\rho C_\mu\frac{k^2}{\varepsilon} \quad (6)$$

The Euler–Lagrange multiphase flow model is used to simulate silt motion; it can describe the interaction between silt and water and the collision of silt particles and its governing equation takes the form[12–14]

$$\frac{\mathrm{d}\vec{u}_p}{\mathrm{d}t}=F_D(\vec{u}-\vec{u}_p)+\frac{\vec{g}(\rho_p-\rho)}{\rho_p}+\vec{F} \quad (7)$$

where $\vec{F}$ is an additional acceleration (force/unit particle mass) term, $F_D(\vec{u}-\vec{u_p})$ is the dragforce per unit particle mass and

$$F_D=\frac{18\mu}{\rho_p d_p^2}\frac{C_D Re}{24} \quad (8)$$

Here, $\vec{u}$ is the fluid phase velocity, $\vec{u_p}$ particle velocity, μ fluid molecular viscosity, ρ fluid density, ρ_p particle density, d_p particle diameter, and C_D drag coefficient. Re is the relative Reynolds number, which is defined as

$$Re=\frac{\rho d_p|\vec{u}_p-\vec{u}|}{\mu} \quad (9)$$

The governing equation incorporates additional forces ($\vec{F}$) in the particle force balance that can be important under special circumstances. The first of these is the virtual mass force, the force required to accelerate the fluid surrounding the particle. This force can be written as

$$F=\frac{1}{2}\frac{\rho}{\rho_p}\frac{\mathrm{d}}{\mathrm{d}t}(\vec{u}-\vec{u}_p) \quad (10)$$

An additional force arises due to the pressure gradient in the fluid

$$F=\left(\frac{\rho}{\rho_p}\right)u_p\nabla u \quad (11)$$

The particle erosion model is used to simulate silt impact action as determined by the erosion rate[15–17]

$$R_{erotion} = \sum_{p=1}^{N_{particles}} \frac{\dot{m}_p C(d_p) f(\alpha) v^{b(v)}}{A_{face}} \quad (12)$$

where $C(d_p)$ is a function of particle diameter, α the impact angle of the particle path with the wall face, $f(\alpha)$ a function of impact angle, v the relative particle velocity, $b(v)$ a function of the relative particle velocity, and A_{face} the area of the cell face at the wall. $C(d_p)$, $f(\alpha)$, and $b(v)$ must be expressed as piecewise-linear, piecewise-polynomial, or polynomial functions in order to define them as part of the wall boundary conditions.

The Euler–Lagrange multiphase flow model and particle erosion model are implemented in the commercial CFD software Fluent 14.5, which was used to conduct all simulations.

Solution method and boundary conditions

The finite volume method is chosen to discretize the governing equations.[18] The SIMPLEC algorithm is used for the pressure–velocity coupling.[19] The second-order upwind difference scheme is adopted for the momentum, turbulence kinetic energy, and dissipation rate equations. The mass flow rate is defined at the inlet boundary and the total pressure at the outlet boundary. The influence of wall roughness is also considered.[20] The standard wall function is used at the near-wall regions.

Results and discussion

Prototype pump

The operating conditions of the prototype pump and silt properties are listed in Table 1.

For the given boundary conditions, the computational head of the prototype pump is $H = 71.82$ m, with an error of only 1.15%. The mathematical model and boundary conditions are therefore acceptable.

Table 1. Operating conditions and silt properties.

Discharge	$Q = 0.95\ m^3/s$
Total head	$H = 71.0$ m
Rotational speed	$n = 960$ r/min
Silt concentration	$\rho = 18.95\ kg/m^3$
Silt diameter	$d = 0.031$ mm
Specific speed	$n_s = 98.7$

The prototype pump is designed for clear water, and the silt abrasion is not considered. The blades of the prototype pump are silt abraded when transporting water containing high silt content. Figure 3 shows the relative velocity on the blade. The inlet relative velocity is found to be large and nonuniform; it is larger on the suction side than on the pressure side, but the outlet relative velocity is smaller on the suction side than on the pressure side. From the erosion rates on the blade (Figure 4), both blade inlet and outlet are severely silt abraded; note that the average erosion rate is larger on the suction side than on the pressure side. Under long-term intensive silt abrasion, local perforations of the blade can easily occur. The particle erosion model defined by equation (12) indicates that, with the same silt conditions, the erosion rate depends on the impact angle and the relative velocity of the particle. Thus, this paper focuses on means of controlling impact angle and relative velocity through changing the blade inlet and outlet shape.

Change blade inlet shape

To control impact angle and relative velocity, this study considers four blade inlet shapes (Figure 5, the latter three are shown compared with the second): Case 1 cuts the blade outer edge from the inlet based on a prototype blade; Case 2 extends the blade inner edge from the inlet; Case 3 decreases the inflow angle of the blade inner edge offsetting the inner edge of the blade inlet with respect to the pressure side; Case 4 increases the inflow angle of the blade inner edge offsetting the inner edge of the blade inlet with respect to the suction side.

For Case 1, the maximum relative velocity decreases and the distribution of the inlet relative velocity becomes uniform. The erosion rate on the pressure side is reduced compared to that of Figure 4(a), especially along the outlet edge; the erosion rate on the suction side is smaller than that seen in Figure 4(b), but the inlet and outlet edges are still seriously abraded. The pump head drops by 0.84 m and the pump efficiency drops by 1.04%.

For Case 2, the silt abrasion on the blade is not suppressed, and the erosion rate at the inlet and outlet is large. The pump head increases by 0.11 m and the pump efficiency drops by 0.93%.

The erosion rate for Case 3 is smaller on the pressure side than that of the prototype pump; however, the outlet edge on the suction side is still seriously abraded. The pump head increases by 0.39 m and the pump efficiency drops by 0.38%.

For Case 4, the maximum relative velocity decreases and the distribution of the inlet relative velocity is uniform. The erosion rate is smaller on the pressure side than that for the prototype pump; the outlet edge on the suction side is seriously abraded; however, the region is small. The pump head and

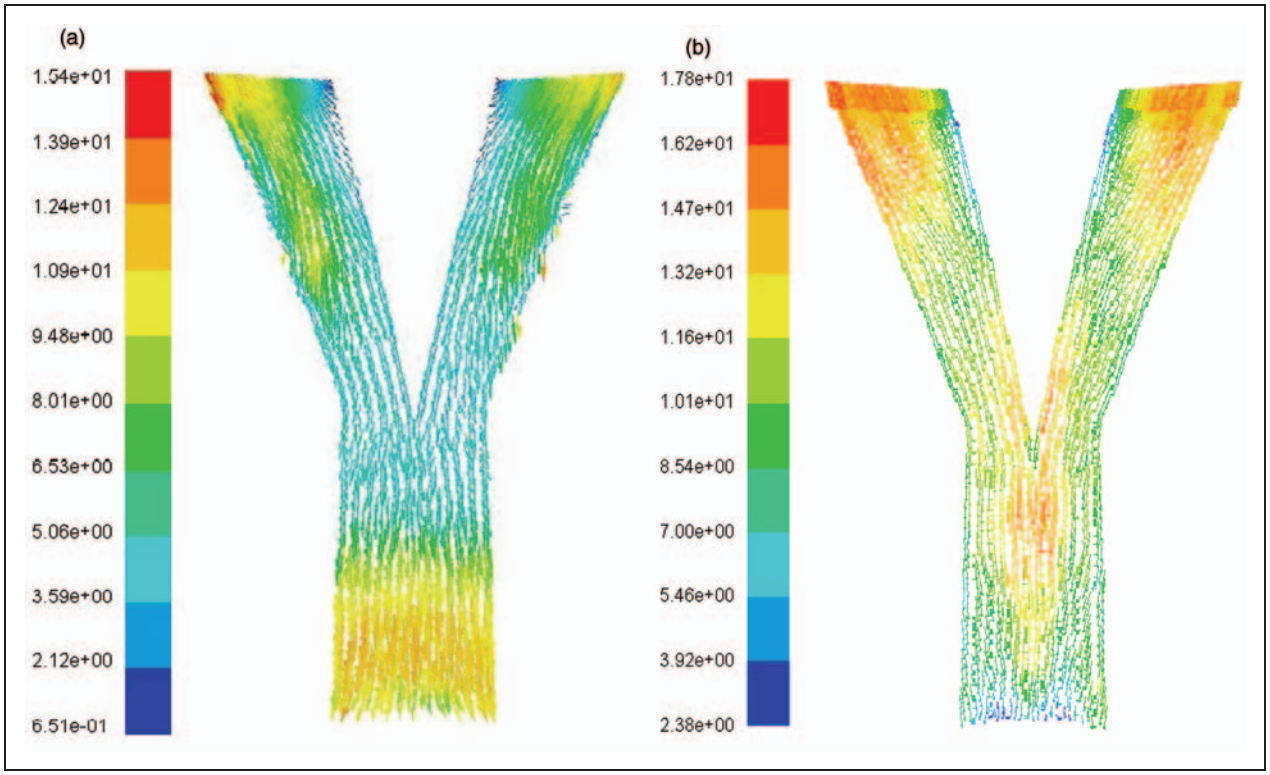

Figure 3. Relative velocity field on the blade (units: m/s): (a) pressure side; (b) suction side.

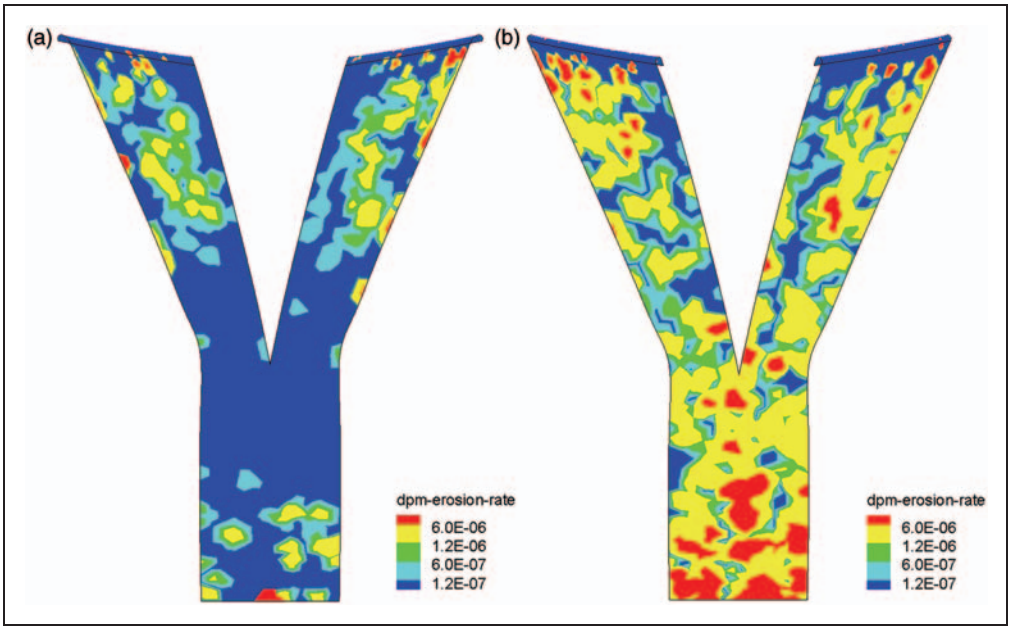

Figure 4. Erosion rate on the pressure and suction side of blade (units: kg/m^2 s^{-1}): (a) pressure side; (b) suction side.

pump efficiency increase by 0.21 m and 0.05%, respectively.

The above analysis shows that under the same silt conditions, the erosion rate on the blade depends on impact angle and relative velocity of particle. Changing the blade inlet shapes could improve flow pattern and silt abrasion on the blade. Cutting the blade outer edge from the inlet, the inlet relative velocity becomes uniform and the erosion rate is reduced; however, the pump head and pump efficiency have also decreased. For Cases 2 and 3, the silt abrasion on the blade is still significant and neither ameliorates abrasion damage. Case 4, with blade outer edge cut away from the inlet and inflow angle of the blade

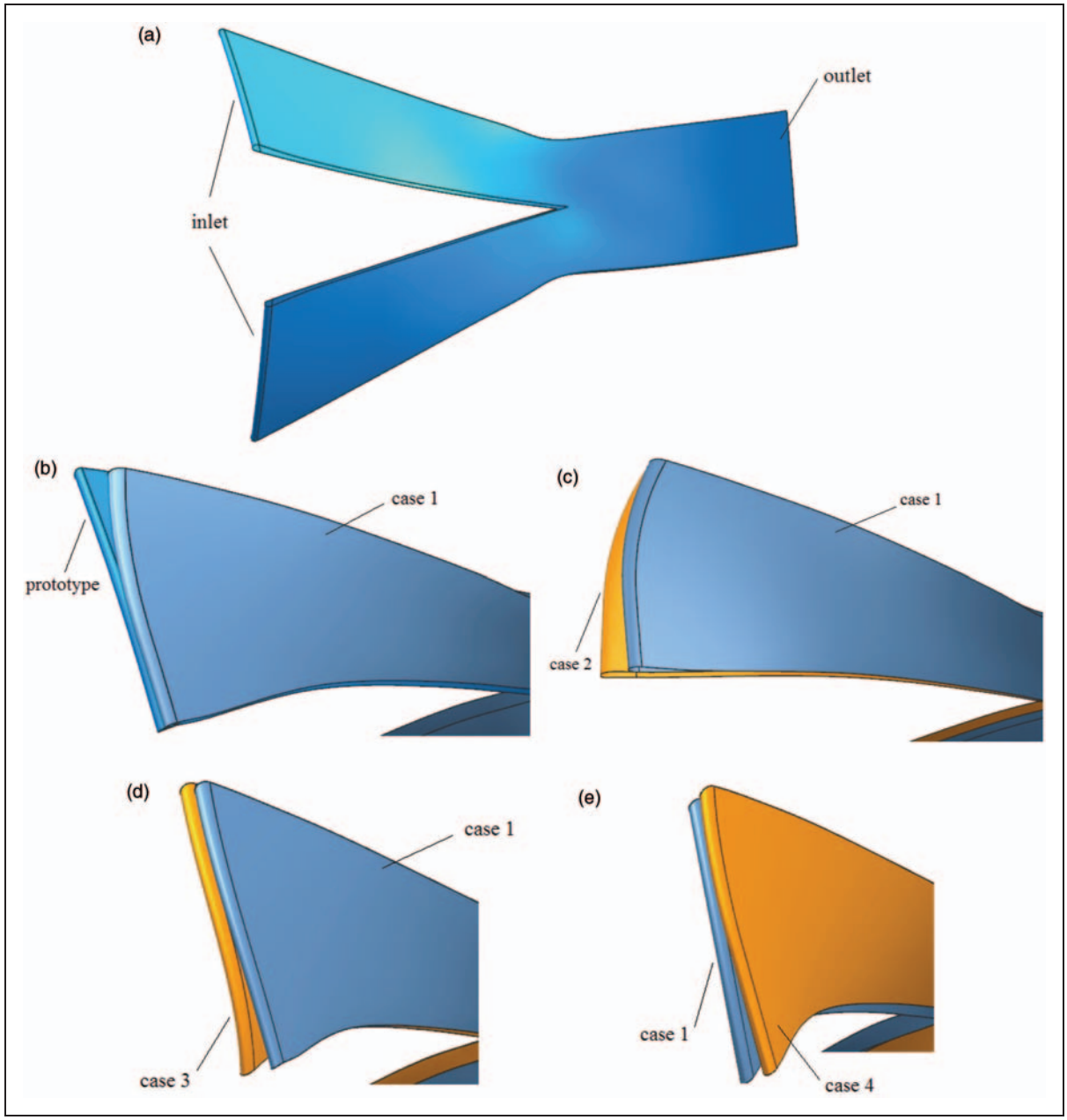

Figure 5. Prototype blade and four blade inlet shapes: (a) prototype blade; (b) Case 1; (c) Case 2; (d) Case 3; (e) Case 4.

inner edge increased, can lower silt abrasion effectively and increase the pump head and pump efficiency slightly. Thus, in this simulation, Case 4 is considered to be an acceptable modification.

Change blade outlet pattern

To control the impact angle and relative velocity, we made four changes to the blade outlet pattern (Figure 6): Case 5 changes the single-outlet passage of the prototype impeller into a symmetrical double-outlet passage with a 10 mm thick plate; Case 6 staggers the sides of the blade of Case 5 by 22.5°; Case 7, which is based on the prototype impeller, retains the pressure side but doubles the thickness of the blade outlet towards the suction side; Case 8, which is also based on prototype impeller, also retains the pressure side but increases the blade outlet thickness by factor 3 towards the suction side.

For Case 5, the erosion rate and the region on the pressure side of the blade are clearly reduced compared to that of Figure 4(a), whereas the silt abrasion on the suction side is not suppressed. The pump head and pump efficiency increase by 0.24 m and 0.84%, respectively.

For Case 6, the erosion rate on the both sides of the blade has clearly declined, with no locally intensive silt abrasion. The pump head and pump efficiency increase by 3.05 m and 1.04%, respectively.

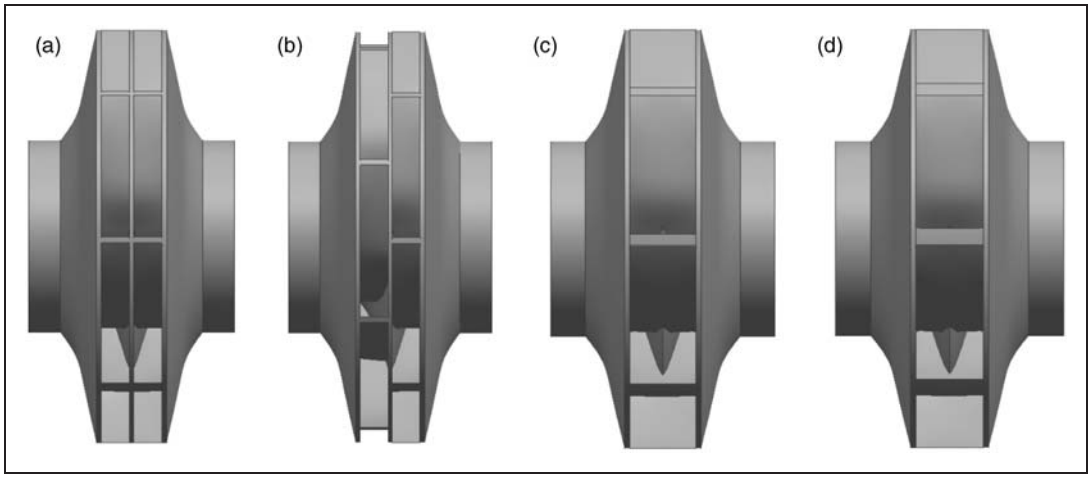

Figure 6. Four blade outlet patterns: (a) Case 5; (b) Case 6; (c) Case 7; (d) Case 8.

For Case 7, the inlet edge on the both sides of the blade is still seriously abraded. The pump head and pump efficiency increase by 1.12 m and 0.35%, respectively.

For Case 8, the erosion rate on the inlet edge of the blade has decreased on the pressure side compared to that in Figure 4(a) whereas on the suction side it is still seriously abraded. The pump head and pump efficiency increase by 2.77 m and 1.31%, respectively.

The above analysis shows that the blade inlet is severely silt abraded, as result of large impact angle and high relative velocity. Comparing the results of the four cases, it can be found that for Cases 5, 7, and 8, the silt abrasion is still serious at either the inlet or outlet, and only Case 6 shows any obvious lowering in silt abrasion with significant simultaneous increases in pump head and pump efficiency. Thus, in this simulation, Case 6 is considered to provide an acceptable adaptation.

The simulation of the combination scheme

We simulated four combination schemes, labeled Cases 9–12, derived from Cases 5–8 in conjunction with Case 4, a changed inlet shape.

For Case 9, the silt abrasion is still serious at the inlet of blade. The pump head and pump efficiency increase by 0.87 m and 1.32%, respectively.

Similarly for Case 10, serious silt abrasion is at the outer edge of blade inlet on the pressure side; the silt abrasion at the outlet edge on the suction side is also serious. The pump head and pump efficiency increase by 3.13 m and 0.95%, respectively.

For Case 11, the distribution of the inlet relative velocity is uniform and the maximum relative velocity decreases compared to that of the prototype. The erosion rate on the pressure sides is reduced obviously; serious silt abrasion appears at the outlet edge on the suction side, but the erosion region is small. In Case 11, the pump head and pump efficiency increase by 1.62 m and 0.29%, respectively.

For Case 12, the local silt abrasion is serious on the pressure side; also the inlet edge on the suction side is seriously abraded. The pump head and pump efficiency increase by 2.42 m and 0.71%, respectively.

The above analysis shows that after changing the blade inlet shape, the inlet relative velocity of the four combination schemes is improved when compared to that of the prototype. Comparing the results of the four cases, only Case 11 lowers silt abrasion on the blade while increasing pump efficiency, albeit slightly. Thus, in this simulation, Case 11 is considered to provide an acceptable adaptation.

Conclusion

Water flow and silt movement in a double-suction centrifugal pump were simulated using an Euler–Lagrange multiphase flow model. Blade erosion rates were predicted using a particle erosion model and the influence of inlet and outlet shapes on silt abrasion were analyzed. The results show:

1. The blade inlet and outlet are severely abraded by silt and the average erosion rate is always larger on the suction side than on the pressure side.
2. Under the same silt conditions, the erosion rate depends on inlet relative velocity and impact angle, which can be controlled by changing the inlet and outlet shapes.
3. Cutting the blade outer edge from the inlet and increasing the inflow angle of the blade inner edge, could effectively control silt abrasion on the blade, and increase the pump head and pump efficiency slightly. Thus, the shape of Case 4 is the most optimal among the four shapes of blade inlet investigated.
4. In optimizing the blade inlet and outlet shape, Cases 6 and 11 are considered acceptable both for improving silt abrasion and maintaining pump head and pump efficiency.

Funding

This investigation was funded by the National Nature Science Foundation of China (Grant No. 51079106) and the Program for New Century Excellent Talents in University (Grant No.NCET-10-0647).

References

1. Tang XL, Tang HF and Wu YL. Simulating and erosion prediction of 3D two phases flow through a turbine runner. *J Eng Thermophys* 2001; 22(1): 51–54.
2. Li Y, Zhu ZC and He ZH. Abrasion characteristic analyses of solid-liquid two-phase centrifugal pump. *J Therm Sci* 2011; 20(3): 283–287.
3. Qian ZD, Wang Y and Gao YY. Numerical simulation of silt abrasion in double-suctions centrifugal pump. *J Hydroelectric Eng* 2012; 31(3): 223–229.
4. Chen HX, Liu WW and Jian W. Impellers of low specific speed centrifugal pump based on the draughting technology. In: *25th IAHR symposium on hydraulic machinery and systems*, *IOP conference series: Earth and environmental science*, Timisoara, Romania, 2010.
5. Qian ZD, Wang Y and Huai WX. Numerical simulation of water flow in an axial flow pump with adjustable guide vanes. *J Mech Sci Technol* 2010; 24(4): 971–976.
6. Blanco M. Numerical flow simulation in a centrifugal pump with impeller-volute interaction. In: *ASME 2000 fluid engineering division summer meeting*, Boston, MA, USA, 11–15 June 2000.
7. Shukla SN and Kshirsagar JT. Numerical experiments on a centrifugal pump. *Am Soc Mech Eng* 2002; 257(2B): 709–720.
8. Chen HX. Research on turbulent flow within the vortex pump. *J Hydrodyn Ser B* 2004; 16(6): 701–707.
9. Launder BE and Spalding DB. The numerical computation of turbulent flows. *Comput Meth Appl Mech Eng* 1974; 3: 269–289.
10. Wang Z and Liu W-m. Two modificatory k-ε turbulence models for turbulent swirling flows. *J Hydrodyn* 2003; 2: 51–57.
11. Yakhot V and Orszag SA. Renormalization group analysis of turbulence. *I: Basic theory*. J Scient Comput 1986; 1(1): 3–11.
12. Qian ZD, Gao YY, Zhang K, et al. Analysis of silt abrasion and shape optimization of blade in a centrifugal pump. *J Power Energy* 2013; 227: 557–566.
13. Wallace MS, Peters JS, Scanlon TJ, et al. CFD-based erosion modeling of multi-orifice choke valves. In: *ASME 2000 fluid engineering division summer meeting*, Boston, MA, USA, 11–15 June 2000.
14. Habib MA, Badr HM, Ben-Mansour R, et al. Erosion rate correlations of a pipe protruded in an abrupt pipe contraction. *Int J Impact Eng* 2007; 34(8): 1350–1369.
15. Edwards JK, McLaury BS and Shirazi SA. Supplementing a CFD code with erosion prediction capabilities. In: *Proceedings of ASME FEDSM'98: ASME 1998 fluids engineering division summer meeting*, Washington, DC, USA, 21–25 June 1998.
16. Haugen K, Kvernvold O, Ronold A, et al. Sand erosion of wear resistant materials: Erosion in choke valves. *Wear* 1995; 186–187: 179–188.
17. Shah SN and Jain S. Coiled tubing erosion during hydraulic fracturing slurry flow. *Wear* 2008; 264: 279–290.
18. Patankar SV. *Numerical heat transfer and fluid flow*. Washington, DC: Hemisphere, 1980, pp.131–134.
19. Patankar SV and Spalding DB. A calculation procedure for heat, mass and momentum transfer in three-dimensional parabolic flows. *Int J Heat Mass Transfer* 1972; 15: 1787–1806.
20. Ishida M, Sakaguchi D and Sun Z. Suppression of rotating stall in vaneless diffuser by wall roughness control. In: *Proceedings of the international conference on pumps and fans*, *ICPE*, Tsinghua, China, 13–16 October 1998, pp.232–241. Beijing: Tsinghua University Press.